HIGH-DRAG REGIMES IN NON-HYDROSTATIC AND/OR ROTATING FLOWS PAST 3-D OBSTACLES

Rita M. Cardoso, Pedro M. A. Miranda, Miguel A. C. Teixeira

University of Lisbon, CGUL, IDL, Lisbon, Portugal
E-mail:rmcardoso@fc.ul.pt

Abstract: Three-dimensional isolated mountains may force high-amplitude internal waves that modify the atmospheric flow in their vicinity. In the case of circular mountains, or whenever their cross-stream extension is small, the establishment of those high-amplitude waves is only possible for a small range of flow parameters, corresponding to a narrow range of values for *Nh/U*. That behaviour has been previously studied for hydrostatic non-rotating flow. This work studies the changes that occur when non-hydrostatic and/or rotating effects are taken into account. Both effects tend to increase horizontal dispersion, reducing the amplitude of standing internal waves. However, when appropriately scaled by the corresponding linear solutions, both non-hydrostatic and rotating flows allow for the establishment of high-drag regimes, qualitatively similar to hydrostatic non-rotating solutions, but at slightly different values of *Nh/U*.

Keywords: *Non-hydrostatic flow, Rotation, High-Drag Regimes*

1. INTRODUCTION

High-drag regimes in stratified flow past obstacles have been the subject of many studies since the late 1970s (e.g. Peltier and Clark, 1979; Clark and Peltier, 1984). In the case of two-dimensional, inviscid, hydrostatic, non-rotating flow, with constant background wind and stability, *Nh/U* is the only relevant non-dimensional parameter. In three-dimensional flows past isolated obstacles, the cross-stream dimensions of the obstacle (*b*) become relevant, leading to a new independent non-dimensional parameter: the horizontal aspect ratio of the mountain (*b/a*, where *a* is the along-stream mountain half-width). In this situation, there is a possibility for horizontal streamline splitting that will eventually lead to a low-drag regime for large mountain heights (Miranda and James, 1992). Stratified rotating flows (Smith, 1979; Ólafsson and Bougeault, 1997; Ólafsson, 2000) will also be controlled by their Rossby number (*U/fa*, where f is the Coriolis parameter) and non-hydrostatic flows will depend on the dimensionless mountain width, *Na/U*. Other complications will arise if the background wind and/or stability profiles vary with height (e.g. Miranda and Valente, 1997; Teixeira, Miranda and Valente, 2004; Teixeira and Miranda, 2006) or with time, or when surface friction is taken into account.

2. NUMERICAL MODEL AND SETUP

The numerical model used is the NH3D mesoscale model developed by Miranda and James (1992) and extended by Rõõm *et al.* (2001). It is a non-hydrostatic model in pressure-based terrain-following coordinates, which has been validated in previous studies. In the experiments shown in the present study, the model is used in its simpler setup, i.e. with no diffusion or surface effects and no water vapour. The model grid, for all cases, consists of 49×49×50 grid points, with horizontal resolution $\Delta x = \Delta y = 0.2a\ km$, and the orography is a circular bell-shaped mountain with a variable halfwidth (*a=1…5km*). Table 1 shows the range of parameters used in the two sets of experiments to be presented.

Table 1: Numerical Experiments

Set	Main Flow Parameters
1	*Nh/U=0.2* to *5; Na/U=5,4,3,2,1.5; U/fa=∞*
2	*Nh/U=0.2* to *5; Na/U=5; U/fa=∞,4,2,1*

Set 1 investigates non-hydrostatic effects in non-rotating flow. For each value of *Na/U=(5,4,3,2,1.5)* a subset of experiments was performed for different mountain heights and, in each case, the model was run for 60 non-dimensional time steps (that is, for *T*=0…60 a/U*). Set 2 investigates rotation effects. In this case *Na/U* is fixed (*Na/U=5*) and *f* is varied to obtain different Rossby numbers (*U/fa=∞,4,2,1*). For each value of

U/fa a subset of experiments was performed for different mountain heights and, in each case, the model was run for *60* non-dimensional time steps (that is, for *T*=0… 60 a/U*). Results will be discussed in the following sections.

3. NON-HYDROSTATIC EFFECTS

The first set of experiments explores a region of the parameter space from small (*Na/U=5*) to strong non-hydrostatic effects (*Na/U=1.5*). Fig. 1 shows the values of the steady state drag in all experiments of this set, except in the case of high-drag flow where the plotted values correspond to the higher non-dimensional drag attained in the corresponding experiment.

For *Na/U=5* results are similar to those obtained by Miranda and James (1992), with maximum non-dimensional drag attained at *Nh/U=1.3-1.5*. As non-hydrostatic effects increase, the drag curve shows a systematic shift to the right, implying that one needs higher mountains (i.e. higher *Nh/U*) to establish the high-drag regime. The low-drag, splitting flow, regime is also established at higher mountain heights and the width of the high drag region is not much affected. As *Na/U* decreases it is not possible to cover the full region of *Nh/U* values, because that would imply using mountain slopes above 1, a situation that cannot be simulated with a sigma coordinate model.

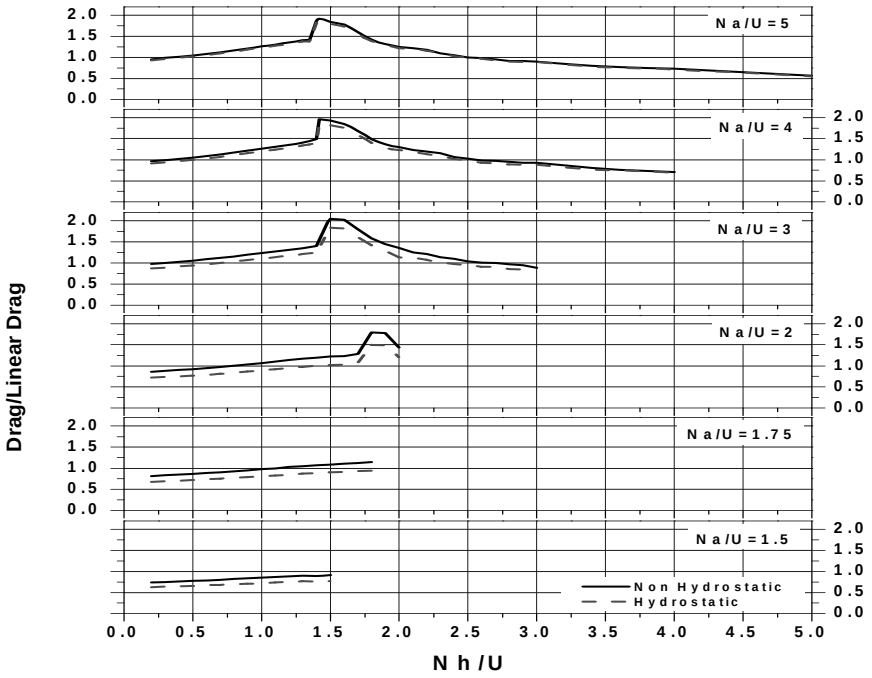

Figure 1: Gravity wave drag in non-rotating flow past circular mountains (set 1). The two curves correspond to two different scalings: drag normalized by the linear hydrostatic drag and by the linear non-hydrostatic drag.

Fig. 2 shows a particular vertical cross-section of the flow in one of the experiments of set 1, for *Na/U=2* and *Nh/U=0.5*, corresponding to a strongly non-hydrostatic regime. Non-hydrostatic effects are clearly identified in Fig. 2, by short downstream waves.

In highly non-hydrostatic high-drag regimes the generation of a stagnation point on the upstream slope occurs even if there is no stagnation point aloft; i.e., if there is no wave breaking, whereas in hydrostatic regimes such a stagnation point is only associated with wave breaking. When *Na/U=2* and *Nh/U=1.7*, a stagnation point is produced after *T*=9* at *x=-1.2a* and no wave breaking was observed during the whole run (*T*=180*). Even when wave breaking is detected, the generation of the upstream stagnation point precedes the generation of the stagnation point aloft. Fig. 3 shows the flow at two instants, one before wave breaking and the other during wave breaking for the case where *Na/U=2* and *Nh/U=1.8*.

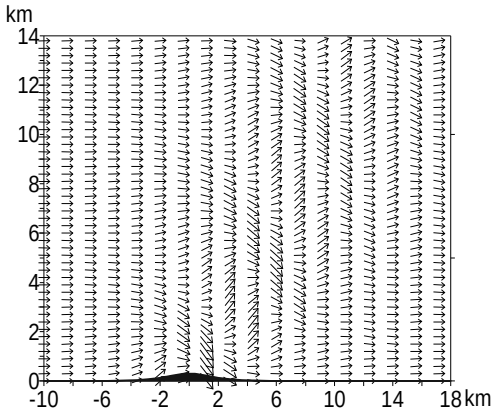

Figure 2: Wind vectors in the *y=0* cross-section, for the experiment with *Na/U=2* and *Nh/U=0.5*.

The emergence of the stagnation point on the upstream slope occurred at *T*=6* and is located at *x=-1.2a*, and remains at this location throughout the whole run. Non-hydrostatic effects are also responsible for an amplification of the reversed flow on the upstream slope.

In this regime as in hydrostatic flows, wave breaking induces de generation of a pair of downstream vortices, but the non-hydrostatic effects have no influence on their dimensions, or on their downstream propagation.

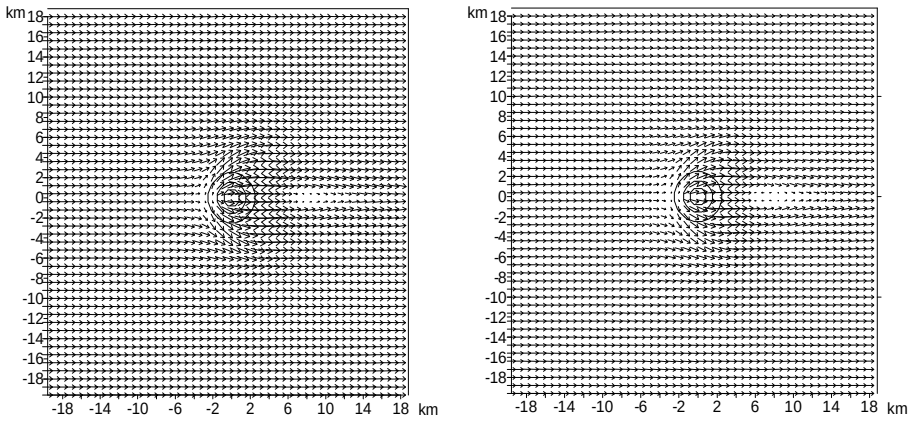

Figure 3: Wind vectors at the lowest model level $\sigma = 0{,}99$ for *T*=55* (before wave breaking) and *T*=60* (during wave breaking). Topography contours at *h/4*, *h/2*, *3h/4*. *Na/U=2* and *Nh/U=1.8*.

4. ROTATION EFFECTS

Fig. 4 presents values of the steady state non-dimensional drag in the experiments of set 2, including rotation. Because of the need to keep all other parameters constant, low values of *U/fa* are used, corresponding to non-geophysical values of *f* (e.g. $f=10^{-3}\ s^{-1}$ for *U/fa=1*). It should also be mentioned that the linear drag value used to scale the drag in Fig. 4 includes rotation effects, using the analytical result of Miranda and James (1992), valid for hydrostatic flow with rotation

$$D = \frac{\pi}{4}\rho_0 NUah_0^2 \left\{ \left[1 + 2\frac{fa}{U} \right] e^{-2\frac{fa}{U}} \right\} \qquad (1)$$

and so high non-dimensional drag values presented in Fig. 4 correspond to modest values of dimensional drag. As for the non-rotating experiments, Fig. 4 also presents a region of high drag flow, which shifts to the right when *U/fa* decreases, indicating that the establishment of these regimes can only occur for higher mountains. An analysis of the flow in the vicinity of the mountain (not shown) reveals the establishment of an inertial oscillation, associated with significant left-right asymmetries in the flow. In these cases, rotation limits the upstream propagation of the disturbances but has no influence on the strength of the downstream flow

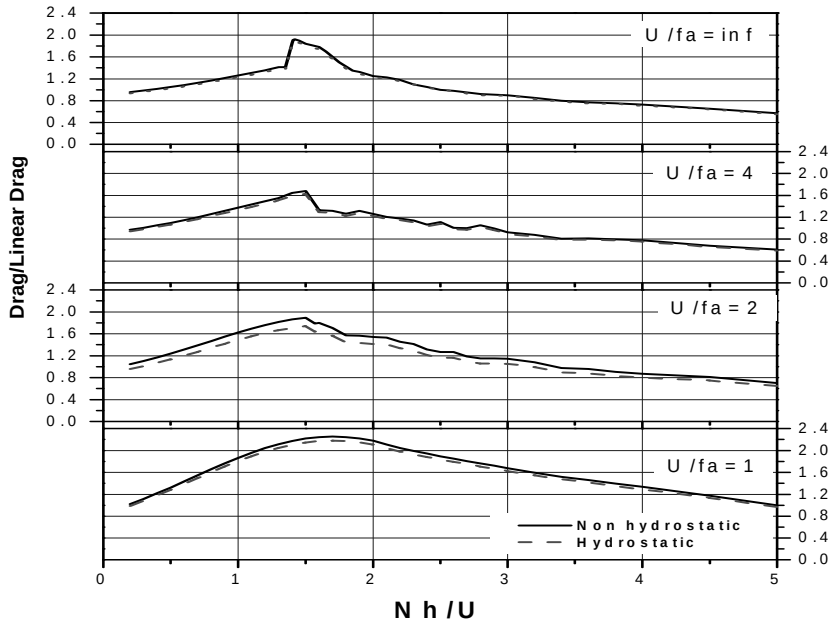

Figure 4: Gravity wave drag in rotating flow past circular mountains (set 2). The two curves correspond to two different scalings: drag normalized by the linear hydrostatic drag and by the linear non-hydrostatic drag.

5. DISCUSSION

Non-hydrostatic effects and rotation influence the establishment of high-drag flow regimes in the neighbourhood of isolated mountains. The changes in the flow produced by those two effects are quite different but their impact in the non-dimensional drag is in the same sense. In both cases one observes a shift of the high-drag regimes towards higher values of the non-dimensional mountain height (*Nh/U*). In spite of that, high (non-dimensional) drag regimes can be maintained for a wide range of both *Na/U* and *U/fa*.

The two sets of experiments, including many dozens of individual simulations, cover only a small sector of the parameter space. In those simulations we opted for keeping the horizontal scale constant, which has the advantage of allowing the model to adequately resolve both the forced and the free oscillation modes. The price to pay was a need to use large (non-geophysical) values of *f*, and consequently reducing the range of upward propagating internal waves in strong rotation regimes (*U/fa=1*). What happens at larger horizontal scales is currently being addressed.

Acknowledgements: *This work was supported by Fundação para a Ciência e Tecnologia (FCT) under project BOSS, contract POCI/CTE-ATM/58932/2004, co-financed by the European Union under program FEDER. R.C. acknowledges the financial support of FCT under Grant SFRH/BPD/26144/2005.*

REFERENCES

Clark, T.L. and Peltier; W.R., 1984: Critical level reflection and the resonant growth of nonlinear mountain waves, *J. Atm. Sci.* , **34**, 1715-1730.

Miranda, P.M.A. and I.N. James ,1992: Non-linear three-dimensional effects on gravity wave drag: spliting flow and breaking waves. *Quart. J. Roy. Meteo. Soc.*, **125**, 1341-1357.

Miranda, P. M. A. and M. A. Valente ,1997: Critical level resonance in three-dimensional flow past isolated mountains. *J. Atm. Sci.*, **54**, 1574-1588.

Ólafsson, H. and P. Bougeault, 1997: The effect of rotation and surface friction on orographic drag. *J. Atm. Sci*., **54**, 193-210.

Peltier, W.R. and T.L. Clark, 1979: The evolution and stability of finite amplitude mountain waves. Part II: Surface wave drag and severe downslope windstorms. *J. Atm. Sci.*, **36**, 1498-1529.

Rõõm, R., P.M.A. Miranda and A.J. Thorpe, 2001: Filtered non-hydrostatic models in pressure-related coordinates. *Quart. J. Roy. Meteo. Soc.*, **127**, 1277-1292.

Smith, R. B., 1979: The influence of the Earth's rotation on mountain wave drag. *J. Atm. Sci*., **36**, 177-180.

Teixeira, M. A. C. and P. M. A. Miranda, 2006: A linear model of gravity wave drag for hydrostatic sheared flow over elliptical mountains. *Quart. J. Roy. Meteor. Soc.*, **132**, 2439–2458.

Teixeira, M. A. C., P. M. A. Miranda and M. A. Valente, 2004: An analytical model of mountain wave drag for wind profiles with shear and curvature. *J. Atmos. Sci.*, **61**, 1040–1054.